# Electronic Structure, Bonding, Spectra, and Linear and Nonlinear Electric Properties of Ti@C-28

**ARTICLE** *in* THE JOURNAL OF PHYSICAL CHEMISTRY A · JULY 2011

Impact Factor: 2.69 · DOI: 10.1021/jp206331n · Source: PubMed



**9 AUTHORS**, INCLUDING:

Robert W. Góra
Wroclaw University of Technology
**54** PUBLICATIONS **717** CITATIONS
SEE PROFILE

Paweł Lipkowski
Wroclaw University of Technology
**27** PUBLICATIONS **432** CITATIONS
SEE PROFILE

Wojciech Bartkowiak
Wroclaw University of Technology
**111** PUBLICATIONS **1,262** CITATIONS
SEE PROFILE

Heribert Reis
National Hellenic Research Foundation
**77** PUBLICATIONS **976** CITATIONS
SEE PROFILE

THE JOURNAL OF PHYSICAL CHEMISTRY A

ARTICLE

pubs.acs.org/JPCA

# Electronic Structure, Bonding, Spectra, and Linear and Nonlinear Electric Properties of Ti@$C_{28}$

Bartłomiej Skwara,[†] Robert W. Góra,[*,†] Robert Zaleśny,[†] Paweł Lipkowski,[†] Wojciech Bartkowiak,[†] Heribert Reis,[‡] Manthos G. Papadopoulos,[*,‡] Josep M. Luis,[§,∥] and Bernard Kirtman[*,⊥]

[†]Theoretical Chemistry Group, Institute of Physical and Theoretical Chemistry, Wrocław University of Technology, Wybrzeże Wyspiánskiego 27, 50-370 Wrocław, Poland

[‡]Institute of Organic and Pharmaceutical Chemistry, The National Hellenic Research Foundation, 48 Vas. Constantinou Avenue, 11635 Athens, Greece

[§]Institute of Computational Chemistry and [∥]Department of Chemistry, University of Girona, Campus de Montilivi, 17071 Girona, Catalonia, Spain

[⊥]Department of Chemistry and Biochemistry, University of California, Santa Barbara, California 93106, United States

Supporting Information

**ABSTRACT:** The potential energy surface (PES) of Ti@$C_{28}$ has been revisited, and the stationary points have been carefully characterized. In particular, the $C_{2v}$ symmetry structure considered previously turns out to be a transition state lying 2.3 kcal/mol above the ground state of $C_{3v}$ symmetry at the MP2/6-31G(d) level. A large binding energy of 181.3 kcal/mol is found at the ROMP2/6-31G(d) level. Topological analysis of the generalized Ti@$C_{28}$ density reveals four bond paths between Ti and carbon atoms of the host. The character of all four contacts corresponds to a partially covalent closed shell interaction. UV−vis, IR, and Raman spectra are calculated and compared with $C_{28}H_4$. The dipole moment and the static electronic and double harmonic vibrational (hyper)polarizabilities have been obtained. Distortion of the fullerene cage due to encapsulation leads to nonzero diagonal components of the electronic first hyperpolarizability $\beta$, and to an increase in the diagonal components of the electronic polarizability $\alpha$ and second hyperpolarizability $\gamma$. However, introduction of the Ti atom causes a comparable or larger reduction in most cases due to localized bonding interactions. At the double harmonic level, the average vibrational $\beta$ is much larger than its electronic counterpart, but the opposite is true for $\alpha$ and for the contribution to $\gamma$ that has been calculated. There is also a very large anharmonic (nuclear relaxation) contribution to $\beta$ which results from a shallow PES with four minima separated by very low barriers. Thus, the vibrational $\gamma$ (and $\alpha$) may, likewise, become much larger when anharmonicity is taken into account.

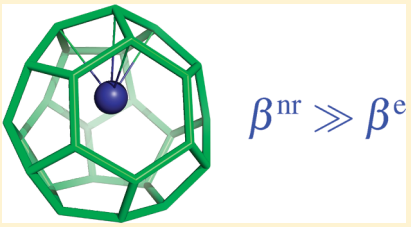


## INTRODUCTION

The ability of fullerenes to entrap atoms was revealed[1] soon after their discovery.[2] Until now, many endohedrally doped fullerenes have been synthesized,[3−5] and since they are a class of conjugated compounds their electric properties have been extensively studied theoretically and experimentally.[6−17] Both atomic and small molecular species, such as transition metal atoms, noble gas atoms, and methane, have been trapped inside carbon cages.[6,18−28] It has been noted that charge transfer and covalent interactions between the fullerene and the encaged species may have a large effect on the electronic structure and properties of the resulting endohedral complex.[6,29−34]

Among the various properties of interest, apart from structure and bonding, are the electronic and vibrational spectra as well as the linear and nonlinear (L&NLO) (hyper)polarizabilities.[35−43] In addition to the pure electronic (hyper)polarizabilities, an important consideration for the endohedral complexes is the contribution due to nuclear motion. Whitehouse and Buckingham predicted an exceptionally large vibrational contribution to the dipole polarizability of $[C_{60}M]^{n+}$ (where M = Li, Na, Mg) at temperatures above 20 K, assuming that the cage-ion potential surface is approximately flat.[44] This also implies that only a small field is required to move the ion from one side of the cage to the other. On the other hand, some of us have recently shown that within the nuclear relaxation approximation, and at 0 K, the vibrational contributions to the polarizability of Li@$C_{60}$ are rather modest.[45] It is of interest to see whether the same is true of Ti@$C_{28}$ and to examine the vibrational hyperpolarizabilities as well. To the best of our knowledge there have been no previous studies of the L&NLO properties of Ti@$C_{28}$. We also report, for the first time, the theoretical UV−vis, IR, and Raman spectra of this system and compare these with the closed shell exohedral molecule $C_{28}H_4$.

In order to elucidate the changes associated with encapsulation of the guest atom, it is helpful to compare selected properties not only with those of the above exohedral complex but also with the host molecule ($C_{28}$). Since all these systems have a relatively

**Received:** July 5, 2011
**Published:** July 26, 2011





dx.doi.org/10.1021/jp206331n | *J. Phys. Chem. A* 2011, 115, 10370–10381

small size, they can be studied using less approximate ab initio methods than in previous work. Although the electronic structure has been investigated, a number of aspects remain worthy of further exploration as will be evident from the following discussion.

$C_{28}$ is one of the smallest fullerenes capable of encapsulating transition metal atoms.[46] Ab initio calculations have shown that it has an $^5A_2$ open shell ground state of $T_d$ symmetry. This molecule can be considered as a superatom with an effective valency of 4, toward both the outside and the inside of the cage. For $C_{28}$ Guo et al.[47] found, at the Hartree−Fock (HF) level of theory and assuming $C_{2v}$ symmetry, a set of low-lying excited electronic states: $^3A_2$, $^3B_1$, and $^1A_1$. These were calculated to lie 1.6, 2.7, and 3.1 eV above the ground state. An isomer of $C_{28}$ with $D_2$ symmetry was also obtained, but it is of considerably higher energy.[46]

Although $C_{28}$ appears to be even more abundant in the supersonic cluster beam produced by laser vaporization than $C_{60}$, it is very reactive. Thus, it can form particularly stable endohedral complexes with tetravalent metal atoms such as Ti, Zr, Hf, and U with relative abundances directly proportional to the size of the encapsulated atom.[46] It was suggested that this trend is associated with better spatial overlap of cage orbitals with the valence orbitals of larger atoms. Another way to chemically stabilize $C_{28}$ is to saturate the four singly occupied, strongly electrophilic, p-like orbitals with four exohedral hydrogen atoms.[48,49] This leads to the tetrahedral $C_{28}H_4$ molecule with a closed shell ground state.

In electronic structure calculations of Ti@$C_{28}$, $T_d$ symmetry has usually been assumed.[50] However, Dunlap et al.[51,52] have shown, through local density functional (LDA) calculations, that the Ti atom is not constrained to the center of the cage. In fact, the Ti atom is attracted significantly toward one of the four carbon atoms positioned in the corners of the tetrahedron (each with a singly occupied valence p-orbital in empty $C_{28}$). This would imply a lower symmetry structure with a 3-fold rotational symmetry. Later on Guo et al. considered a $C_{2v}$ symmetry structure.[47] One of the objectives of this work is to perform more accurate ab initio calculations to characterize the $C_{2v}$ and $C_{3v}$ stationary points. Furthermore, an "atoms in molecules" (AIM) bonding analysis is carried out on the global minimum structure.

The remainder of this paper is organized in three sections. In the following section we present our Computational Methods. The Results and Discussion section is next, followed by the Conclusions.

## COMPUTATIONAL METHODS

**Electronic Properties.** The structural and static electronic electric properties (dipole moment, polarizability, first- and second-order hyperpolarizability) of the studied systems were computed using second-order Møller−Plesset perturbation theory with a restricted Hartree−Fock zero-order wave function, i.e., either closed shell (RMP2) or open shell (ROMP2) as appropriate. For the open shell case we used McWeeny and Diercksen canonicalization parameters.[53] For the selected properties of closed shell systems, we used also the Kohn−Sham formulation of density functional theory (KS-DFT) with the BLYP, B3LYP, and CAM-B3LYP exchange-correlation functionals. The choice of the ROHF reference wave function in calculations of $C_{28}$ was mainly due to high spin contamination in the unrestricted Hartree−Fock (UHF) wave function and the large weight of the ROHF configuration in the configuration interaction (CI) wave function reported by Zhao and Pitzer.[54] It should be noted, however, that the arbitrariness in construction of the canonical Fock matrix leads to nonuniqueness in the perturbation theories based on the ROHF zero-order wave function. Nevertheless, the resulting potential energy surfaces and other property surfaces are expected to be highly parallel. There is an excellent recent discussion of this subject by Glaesemann and Schmidt.[55] It should also be noted that for Ti@$C_{28}$ we observed UHF instabilities of the RHF wave function. Although such instabilities and high spin contamination usually indicate a fundamental shortcoming of the single determinant wave function description, previous studies suggest that, in the case of polycyclic aromatic hydrocarbons and linear polyenes, the R(O)MP2 method will yield energies and electric properties in relatively good agreement with highly electron-correlated methods,[56−58] and the same may be expected for the systems studied here. Finally, for Ti@$C_{28}$ we performed single point CASSCF calculations to obtain several low-lying singlet and triplet states using various active spaces and a small atomic natural orbital basis set. These calculations confirmed that the ground state is $^1A_1$ and that it is well represented by the SCF wave function (the weight of the RHF configuration in all the CASSCF wave functions was always greater than 80% and the weights of the individual remaining configurations were always smaller than 1%).

Since the ground state of Ti@$C_{28}$ is a closed shell singlet, and Ti is a 3d transition element, we believe that there is little need to account for relativistic effects in our calculations. Such an assumption is supported by recent studies of TiC in which the effect of scalar relativity on the computed spectroscopic constants including dipole moments was found to be quite small.[59] This greatly simplifies the computational treatment of Ti@$C_{28}$ in comparison with that of endohedral complexes with heavier tetravalent atoms.

Structural parameters were estimated using either the MP2 method with the 6-31G(d,p) basis set or KS-DFT with 6-31+G(d,p); all L&NLO property calculations (including electronic and vibrational spectra) were carried out with the 6-31+G(d,p) basis. MP2 calculations of electric properties using larger basis sets are cumbersome due to the size of the systems studied here. Therefore, in order to investigate the effect of basis set extension, we used the KS-DFT method with the B3LYP functional. The data reported in Table 1 indicate that the static electronic electric properties of Ti@$C_{28}$, computed here by means of the MP2 and B3LYP methods, with the 6-31+G(d) basis set, are consistent with each other and can be regarded as being of semiquantitative accuracy.

The static electronic electric properties reported in this study were estimated by means of the finite-field (FF) method with either the Rutishauser−Romberg (RR)[60] or Kurtz et al.[61] procedure.

**Table 1. Selected Components of the Static Electronic Electric Dipole Moment and (Hyper)polarizabilities (in au) of Ti@$C_{28}$ Estimated Using the B3LYP and MP2 Methods with Various Basis Sets**[a]

| | $\mu_z$ | $\alpha_{zz}$ | $\beta_{zzz}$ | $\gamma_{zzzz}$ |
|---|---|---|---|---|
| MP2/6-31G(d) | 0.921 | 220.34 | −262.9 | $12.5 \times 10^3$ |
| MP2/6-31+G(d) | 1.088 | 258.83 | 23.1 | $103.7 \times 10^3$ |
| B3LYP/6-31+G(d) | 1.214 | 250.88 | 38.4 | $83.3 \times 10^3$ |
| B3LYP/aug-cc-pVDZ | 1.207 | 252.73 | 52.8 | $78.2 \times 10^3$ |
| B3LYP/aug-cc-pVTZ | 1.179 | 252.56 | 55.3 | $78.0 \times 10^3$ |

[a] Electric properties were estimated from fits of finite-field calculations using the Rutishauser−Romberg approach. The MP2/6-31G(d) equilibrium geometry was assumed in all calculations.

These properties are defined in terms of a Taylor series expansion of the energy in an external electric field (using the Einstein summation notation):

$$E(F) = E(0) - \mu_i F_i - \frac{1}{2!}\alpha_{ij}F_iF_j - \frac{1}{3!}\beta_{ijk}F_jF_kF_l - \frac{1}{4!}\gamma_{ijkl}F_iF_jF_kF_l + \ldots \quad (1)$$

$E(0)$ is the field-independent energy, while $\mu_i$, $\alpha_{ij}$, $\beta_{ijk}$, and $\gamma_{ijkl}$ are the components of the dipole moment, polarizability, first hyperpolarizability, and second hyperpolarizability tensors, respectively. All off-diagonal tensor elements were computed using the treatment of ref 61 with a base field of 0.001 au.

All diagonal property values were computed by employing the more accurate RR approach. For the latter a number of field strengths of magnitude $2^mF$ were used, where $m$ denotes a set of consecutive integers and $F = 0.0001$ au. We have found that the region of stability falls in the range $F = 0.0008-0.0016$ au, which is why the base field 0.001 au was used for the off-diagonal elements.

For the average properties we used

$$\overline{\alpha} = \frac{1}{3}\sum_{i=x,y,z}\alpha_{ii} \quad (2)$$

$$\overline{\beta} = \sum_{i=x,y,z}\frac{\mu_i\beta_i}{|\mu|} \quad (3)$$

where

$$\beta_i = \frac{1}{5}\sum_{j=x,y,z}(\beta_{ijj} + \beta_{jij} + \beta_{jji}) \quad (4)$$

and

$$\overline{\gamma} = \frac{1}{5}\sum_{ij=x,y,z}\gamma_{iijj} \quad (5)$$

The calculated UV−vis, IR and Raman spectra were plotted utilizing the open-source GaussSum routines.[62]

**Vibrational Contributions to Electric Dipole (Hyper)-Polarizabilities.** The total (hyper)polarizability for the nonrotating molecule can be divided into two contributions:[63]

$$P = P^{e} + P^{vib} \quad (6)$$

where $P^{e}$ and $P^{vib}$ denote the electronic (including the zero-point vibrational averaging (zpva) correction) and pure vibrational properties, respectively. For the sake of simplicity we will drop the superscript "e" hereafter, unless it is necessary to distinguish electronic from vibrational contributions, and ignore the usually small zpva correction. $P^{vib}$ can be expressed as the sum of two terms:[63]

$$P^{vib} = P^{nr} + P^{c\text{-}zpva} \quad (7)$$

where $P^{nr}$ is the nuclear relaxation contribution associated with the change in clamped nucleus electronic (without zpva) properties due to the change in equilibrium geometry induced by the field. $P^{c\text{-}zpva}$ (for notation see ref 64) is associated with the effect of the field-induced geometry relaxation on the corresponding zpva correction to the clamped nucleus electronic property values.[65] The latter term contains all remaining vibrational contributions not included in $P^{nr}$. It is usually smaller than the nuclear relaxation contribution[66,67] and is not computed here. In the Bishop−Kirtman square bracket nomenclature the static ($\omega = 0$) $P^{nr}$ properties are given by[68]

$$\alpha^{nr} = [\mu^2]^{0,0}_{\omega=0} \quad (8)$$

$$\beta^{nr} = [\mu\alpha]^{0,0}_{\omega=0} + [\mu^3]^{1,0}_{\omega=0} + [\mu^3]^{0,1}_{\omega=0} \quad (9)$$

$$\gamma^{nr} = [\alpha^2]^{0,0}_{\omega=0} + [\mu\beta]^{0,0}_{\omega=0} + [\mu^2\alpha]^{0,1}_{\omega=0} + [\mu^2\alpha]^{1,0}_{\omega=0} + [\mu^4]^{2,0}_{\omega=0} + [\mu^4]^{0,2}_{\omega=0} + [\mu^4]^{1,1}_{\omega=0} \quad (10)$$

The individual terms $[\,]^{n,m}$, where $n$ and $m$ denote the order of electrical anharmonicity and mechanical anharmonicity, respectively, may be computed from energy, dipole moment, and (hyper)-polarizability derivatives.[68]

The Bishop−Kirtman perturbation method, and the related nr treatment, is appropriate in the nonresonant regime wherein it is assumed that the laser optical frequencies may be neglected in comparison with electronic transition frequencies. Recently, a response formalism for computation of the terms that are thereby omitted has been presented.[69] However, it has now been shown that these missing terms vanish at both the static and infinite optical frequency limits, which are the cases studied here.[70]

The vibrational contributions to the (hyper)polarizabilities were computed assuming the double harmonic approximation (in which only $[\,]^{0,0}$ terms are retained in eqs 8−10). In order to make a preliminary assessment of the anharmonicity contributions to hyperpolarizability, we also used the finite-field approach proposed by Bishop, Hasan, and Kirtman[71] and developed by Luis et al.[72]

All vibrational contributions to the (hyper)polarizabilities were estimated within the KS-DFT approach with the BLYP, B3LYP, and CAM-B3LYP exchange-correlation functionals[73−75] (as implemented in the Gaussian 09[76] suite of programs) and the 6-31+G(d) basis set.

## RESULTS AND DISCUSSION

**Structural Properties.** *$C_{28}$.* The equilibrium structure of the $^5A_2$ ground state of $C_{28}$ was obtained at the ROMP2/6-31G(d) level of theory, assuming $T_d$ symmetry and using analytical energy gradients as implemented in the GAMESS (US) package.[77] As pointed out by Guo et al.,[47] this structure has only three symmetry-distinct bond lengths (Figure 1). $R_1$ denotes the bond bridging the six-membered rings, $R_2$ is the bond within six-membered rings, and $R_3$ is the edge shared by two pentagons in the triplet of pentagons. In Table 2 we compare our results for the bond lengths with those obtained by Guo et al. at the HF/DZ level (probably UHF, though not specified).[47] Electron correlation influences the $C_{28}$ structure significantly. In comparison with ROHF our ROMP2 $R_1$ and $R_3$ bonds are somewhat shorter, while the $R_2$ bond is elongated. For the sake of comparison we report also the corresponding UMP2 values, although these are less reliable due to high spin contamination.

*Ti@$C_{28}$.* The equilibrium structure of Ti@$C_{28}$ (see Figure 2), obtained at the RMP2/6-31G(d) level of theory, has $C_{3v}$ symmetry. Guo et al.[47] reported a symmetry lowering to $C_{2v}$, but we found that the structure proposed and analyzed in their paper is, in fact, a first-order saddle point that lies 2.3 kcal/mol above the

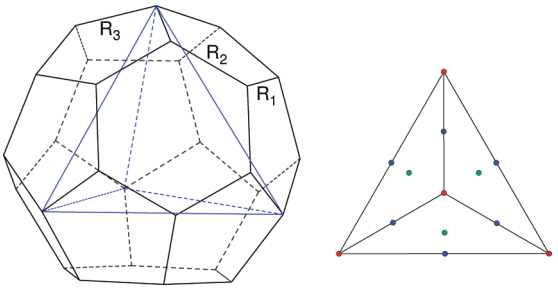


**Figure 1.** Structure of $C_{28}$ with inscribed tetrahedron indicating its $T_d$ point group symmetry (left). On the right we plot the projection of the tetrahedron showing schematically the relevant positions of the guest atom and the corresponding point group symmetries of the endohedral complex. In the case of Ti@$C_{28}$ the red dots correspond to $C_{3v}$ minima, the green dots on the faces of tetrahedron indicate the $C_{3v}$ transition states, and the blue dots represent the $C_{2v}$ transition states.

**Table 2. Structural Parameters of $C_{28}$ ($T_d$)[a]**

| | $R_1$ | $R_2$ | $R_3$ |
|---|---|---|---|
| HF/DZ[b] | 1.538 | 1.397 | 1.482 |
| ROHF/6-31G(d) | 1.511 | 1.403 | 1.475 |
| UMP2/6-31G(d) | 1.419 | 1.407 | 1.443 |
| ROMP2/6-31G(d) | 1.499 | 1.440 | 1.434 |

[a] Bond lengths, defined in Figure 1, are in Angstroms. [b] Guo et al.[47]

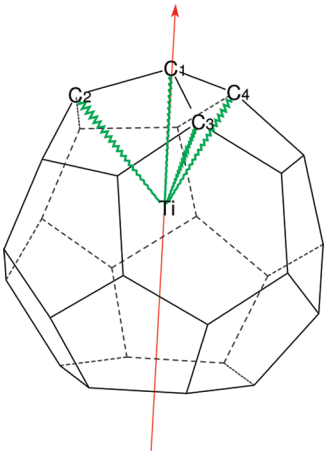


**Figure 2.** Structure of Ti@$C_{28}$. The principal symmetry axis $C_3$ ($z$) is shown in red, and the schematic QTAIM bond paths are indicated in green. See text for the discussion.

global minimum. The $C_{28}$ cage in the complex has nine distinguishable bond lengths with the Ti atom on the $C_3$ axis, 2.070 Å away from the $C_1$ carbon. Apart from the stationary points just mentioned, there are saddle points of $C_{3v}$ and $T_d$ symmetry, which are reported in the Supporting Information. These are located 7.1 and 47.8 kcal/mol, respectively, above the $C_{3v}$ global minimum (MP2/6-31G(d) estimates).

In order to explain how the different stationary points are interconnected on the potential energy surface, we would like to draw the reader's attention to the symmetry elements of an isolated $C_{28}$ cage shown in Figure 1. This cage has the shape of a regular tetrahedron with four carbon atoms at the vertices, and

**Table 3. AIM Topological Properties (in au) of Ti···C Bond Critical Points in the Ti@$C_{28}$ Endohedral Complex**

| BCP | $R_{Ti\cdots C}$ | $\rho(r_{BCP})$ | $\nabla^2\rho(r_{BCP})$ | $V(r_{BCP})$ | $G(r_{BCP})$ | $H(r_{BCP})$ | $\varepsilon(r_{BCP})$ |
|---|---|---|---|---|---|---|---|
| Ti···$C_1$ | 2.069 | 0.096 | 0.283 | −0.126 | 0.098 | −0.028 | 0.000 |
| Ti···$C_{2-4}$ | 2.087 | 0.089 | 0.294 | −0.120 | 0.097 | −0.023 | 0.719 |

the central point (which we assume in this discussion to be the origin) has $T_d$ symmetry. For the endohedral complex with Ti atom at the origin, our calculations indicate that this point on the potential energy surface (PES) is a third-order saddle point with triply degenerate imaginary frequencies of $t_2$ symmetry. The three normal modes correspond to displacements of Ti along the three $C_2$ symmetry axes passing through the origin and bisecting two opposite edges of the tetrahedron. This stationary point is a transition state that connects six equivalent $C_{2v}$ symmetry stationary points and lies 45.5 kcal/mol above them. We have already pointed out that the $C_{2v}$ stationary points, in turn, are first-order transition states that connect two neighboring $C_{3v}$ minima. There are four such minima, each of which may be generated by a displacement of the Ti atom from the origin along one of the four $C_3$ axes that pass through the vertex carbon atoms. In addition, there are four $C_{3v}$ stationary positions where the Ti atom is displaced in the opposite direction along the $C_3$ axis. These are second-order saddle points with imaginary frequencies of e symmetry (in the $C_{3v}$ point group), and they connect three neighboring $C_{3v}$ minima that lie in a plane parallel to a face of the tetrahedron. The saddle point is located 7.1 kcal/mol above the minima.

Although we report only the most accurate MP2/6-31G(d) results, the location of all the stationary points and their character was confirmed via fully analytical Hessian calculations using the HF and B3LYP methods. In the case of MP2 calculations we performed either analytical or seminumerical (four point) Hessian calculations. Furthermore, we performed intrinsic reaction coordinate (IRC) calculations at the HF/6-31G(d) level for all saddle points in order to determine the minimum energy paths and confirm our assignment.

**Bonding Properties, Electronic Spectra, and Vibrational Spectra of Ti@$C_{28}$.** *Binding Energy and Nature of Interactions.* The binding energy (BE) of the endohedral complex in the $^1A_1$ ground state with respect to isolated $^5A_2$ $C_{28}$ and $^3F_2$ Ti ([Ar]$d^2s^2$) has been reported by Dunlap et al.[51] at the LDA/VTZP level of theory and by Guo et al.[47] at the HF/DZ level of theory. In the former case, the value is 258.3 kcal/mol, whereas in the latter it is −18.4 kcal/mol. This difference is remarkable, even taking into account that LDA tends to overestimate the BE contrary to the HF approximation, which usually underestimates this property. Our value for the binding energy of Ti@$C_{28}$ is 215.4 kcal/mol at the R(O)MP2/6-31G(d) level of approximation assuming McWeeny and Diercksen canonicalization parameters. When the Boys and Bernardi counterpoise correction[78] for the basis set superposition error at the equilibrium geometry is taken into account, this value is reduced to 181.3 kcal/mol, which is our best estimate.

Such a large value of BE indicates strong chemical bonding between Ti and $C_{28}$. In order to gain more insight into the nature of this interaction, we performed an AIM analysis (see Table 3), which is based on the topology of the electron density.[79−82] Our calculations were performed with the AIM2000 program[83] using the generalized MP2 electron density to characterize the four

bond paths formed between Ti and carbon atoms $C_1-C_4$ (indicated schematically in green in Figure 2). The Ti···$C_1$ interaction differs significantly from the remaining Ti···$C_{2-4}$ contacts, which are identical by symmetry. The distance to $C_1$ is shorter by about 0.02 Å, and as expected, the electron density at the bond critical point $\rho(r_{BCP})$ is greater (0.096 au versus 0.089 au). The larger value of the ellipticity, $\varepsilon(r_{BCP})$, for the $C_{2-4}$ bond paths implies greater distortion of the cylindrical shape of the electron density distribution, as in the case of double bonds. In fact, the magnitude of the ellipticity in this case is larger than the corresponding $\varepsilon(r_{BCP})$ of ethylene.

An AIM analysis allows one to classify interactions as covalent, closed shell, or somewhere in between, i.e., partially covalent, based on the Laplacian of the electron density $\nabla^2\rho(r_{BCP})$ and on the total energy density at the BCP ($H(r_{BCP})$). The latter is the sum of local kinetic ($G(r_{BCP})$) and potential energy ($V(r_{BCP})$) densities. From the positive values of $\nabla^2\rho(r_{BCP})$ obtained for all Ti···C interactions, we conclude that the interactions are of closed shell character.[80] However, the values of $H(r_{BCP})$ are slightly negative, indicating that the closed shell character is only partial and, therefore, that the four Ti···C interactions may be described as partially covalent in nature.[84] The molecular graph of Ti@$C_{28}$ is available in the Supporting Information.

*UV−Vis, IR, and Raman Spectra of Ti@$C_{28}$ and Comparison with $C_{28}H_4$.* Theoretical studies of the excited electronic states of $C_{28}$ and its endohedral complexes are scarce and usually limited to the analysis of orbital energy differences, particularly involving frontier orbitals.[50−52,85] The most extensive analysis of the low-lying electronic states of $C_{28}$ is that performed by Zhao and Pitzer.[54] These authors carried out limited single and double spin−orbit CI calculations with improved virtual orbitals and found that, although the $^5A_2$ ground state is very well represented by the HF wave function, most of the excited states have large CI mixing. To our knowledge there are no existing theoretical investigations of excited electronic states of Ti@$C_{28}$ other than a single density of states calculation,[85] nor are there any experimental UV−vis spectra of this system. The same is true of $C_{28}H_4$. In this work we fill that lacuna by calculating the UV−vis spectra of Ti@$C_{28}$ and its simplest exohedral counterpart ($C_{28}H_4$) within adiabatic time-dependent density functional theory (TDDFT).

A schematic spectrum for the first 200 states of Ti@$C_{28}$ was determined using the BLYP, B3LYP, and CAM-B3LYP functionals and the 6-31+G(d,p) basis set at the MP2/6-31G(d) optimized geometry. The results shown in Figure 3 were obtained by convolution of the line positions with Gaussian functions assuming a full width at half-maximum of 3000 $cm^{-1}$. Our choice of the BLYP density functional was dictated by a previous report indicating a reasonable performance of nonhybrid functionals for prediction of electronic absorption spectra of fullerenes.[86] One should note, however, that TDDFT is applicable, in general, only to low-lying excited states that do not have appreciable double-excitation or charge-transfer character. In order to get some feeling for the effect of different functionals, we decided to compare with hybrid B3LYP and the CAM-B3LYP variant that has improved asymptotic behavior. All three functionals predict qualitatively similar spectra with the same origin of the most intense lines. However, the hybrid functionals predict that the main features will be slightly shifted toward shorter wavelength and also predict larger shifts of the less intense lines in the shoulder. Since there are no experimental data for comparison, in the following discussion we focus on the BLYP results and comment on the nature of the observed shifts.

The first excited state, which mainly involves the HOMO−LUMO transition, occurs at about 650 nm (1.909 eV). It is dipole forbidden like the majority of electronic transitions above 300 nm. The fact that the electronic spectrum is quenched in the long wavelength region is not surprising. This is, in fact, quite common in similar systems and is partially due to the high symmetry. For example, in the $C_{60}$ fullerene there are sharp bands at about 213, 257, and 329 nm, but only weak features at higher wavelengths.[87]

The most intense lines in Ti@$C_{28}$ appear at about 232 and 236 nm and are of $A_1$ and E symmetry, respectively. For the sake of analysis recall that $C_{28}$ has tetrahedral symmetry with four carbon atoms at the vertices and a benzene-like hexagon of carbon atoms located at the four faces. It is convenient to adopt this tetrahedral structure as a basis for describing the molecular orbitals (MOs) of the encapsulated Ti system.[54] A linear combination of the vertex carbon p atomic orbitals (AOs) leads to $a_1$ and $t_2$ MOs. Under reduced $C_{3v}$ symmetry, the latter splits into an $a_1$ plus an e pair. The main component of the 232 nm peak is due to a transition from the vertex p−$\pi$ bonding MO of $a_1$ symmetry, with a significant contribution of Ti $d_{z^2}$, to the $\pi^*$ ($a_1$) MO composed of carbon p−$\pi$ AOs on the hexagonal and pentagonal faces of $C_{28}$. On the other hand, the 236 nm $^1E$ transition is mainly due to excitation from the doubly degenerate vertex p−$\pi$ + Ti d (e) orbitals to hexagonal $\pi^*$ MOs of $a_1$ and $a_2$ symmetry (see Figure 3a). These $A_1$ and E lines are shifted toward shorter wavelength by about 20 and 35 nm in the cases of B3LYP and CAM-B3LYP, respectively. Thus, the observed shift is related to the proportion of exact exchange included in the hybrid functional (the amount of exact HF exchange in CAM-B3LYP increases throughtout the long-range region). One observes also a corresponding shift of the 300 nm peak combined with a significant increase of intensity. This is mainly due to several E and $A_1$ symmetry transitions similar in nature to the main feature (see Supporting Information for a more detailed version of the plot).

In order to further elucidate the effect of Ti encapsulation on the electronic spectrum of the endohedral complex, we investigated, at the same level (BLYP and B3LYP), the simplest analogous closed shell exohedral system, namely tetrahedral $C_{28}H_4$. Our resultant schematic UV−vis spectra are shown in Figure 3b. Interestingly, they are quite similar to those of the endohedral complex. Now, however, the two most intense lines in Ti@$C_{28}$ ($A_1$ + E) combine into a single line of $T_2$ symmetry with roughly the same oscillator strength as $A_1$ or E individually, and the line is shifted to shorter wavelength (217 and 198 nm in the cases of BLYP and B3LYP, respectively). The main components of these transitions are due to excitations from the doubly degenerate p−$\pi$ (e) orbitals located on the C−C bonds joining two hexagons to $\pi^*$ MOs of $t_2$ symmetry (see Figure 3b). On the other hand, there is also a $T_2$ transition at 328 nm, which is largely quenched in the spectrum of the endohedral complex, and another at 295 nm corresponding to the 282 nm peak of Ti@$C_{28}$ (BLYP results). Although the differences between the B3LYP and BLYP functionals are qualitatively the same as in the case of Ti@$C_{28}$, we note that the wavelength shifts as well as the observed increase of intensity are more pronounced for $C_{28}H_4$. Indeed, a comparison of the theoretical spectra of the endohedral and exohedral species indicates that the main effect associated with encapsulation of the Ti atom is the small red shift of the main feature and the associated increase of its intensity by roughly 20%. The latter arises mainly from an increased number of allowed, small intensity transitions due to the lowered

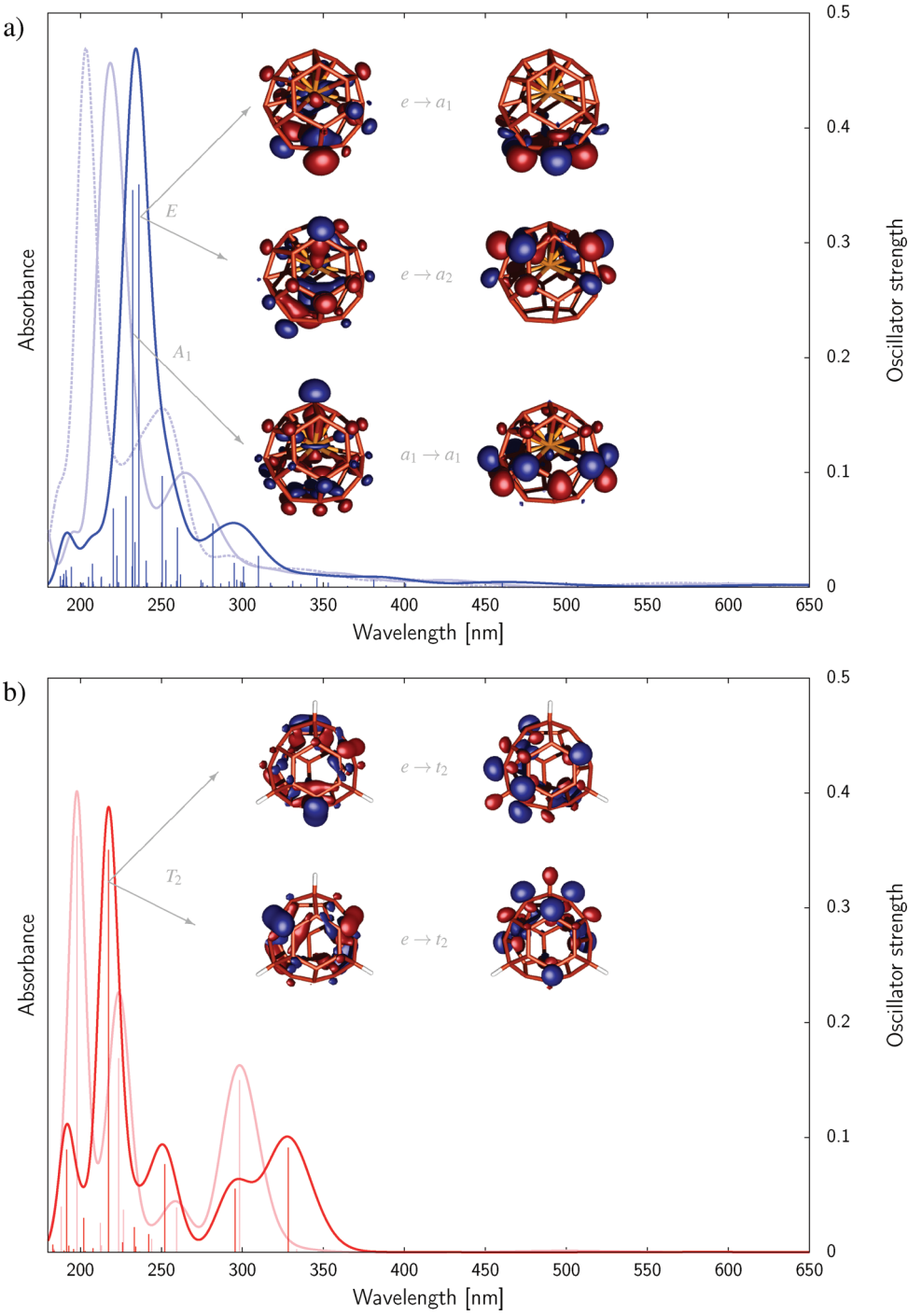


**Figure 3.** UV−vis spectra of Ti@$C_{28}$ (a) and $C_{28}H_4$ (b) computed by means of the adiabatic TDDFT method using BLYP (solid dark lines), B3LYP (solid light lines), and CAM-B3LYP (dashed lines) exchange-correlation functionals and 6-31+G(d,p) basis set at the optimized MP2/6-31G(d,p) geometry.

symmetry. Unfortunately, there are no experimental data available for comparison.

Besides the electronic spectra we have also estimated the spectral frequencies, as well as IR and Raman intensities for the fundamental vibrations of Ti@$C_{28}$ and $C_{28}H_4$. These calculations were done using the B3LYP and CAM-B3LYP functionals with the 6-31+G(d) basis set. The resulting spectra, obtained by convolution of the line positions with Lorentzian curves assuming a full width at half-maximum of 10 $cm^{-1}$, are shown in Figure 4. Our numerical values as well as an assignment of the symmetry species of the corresponding vibrations can be found in the Supporting Information.

An extensive assessment of different DFT functionals for the prediction of vibrational frequencies, IR intensities, and Raman activities of 122 molecules has been carried out by Jiménez-Hoyos et al.[88] They found that B3LYP and, to a slightly lesser extent, CAM-B3LYP performed very well for these quantities, if basis sets containing polarization and diffuse functions were

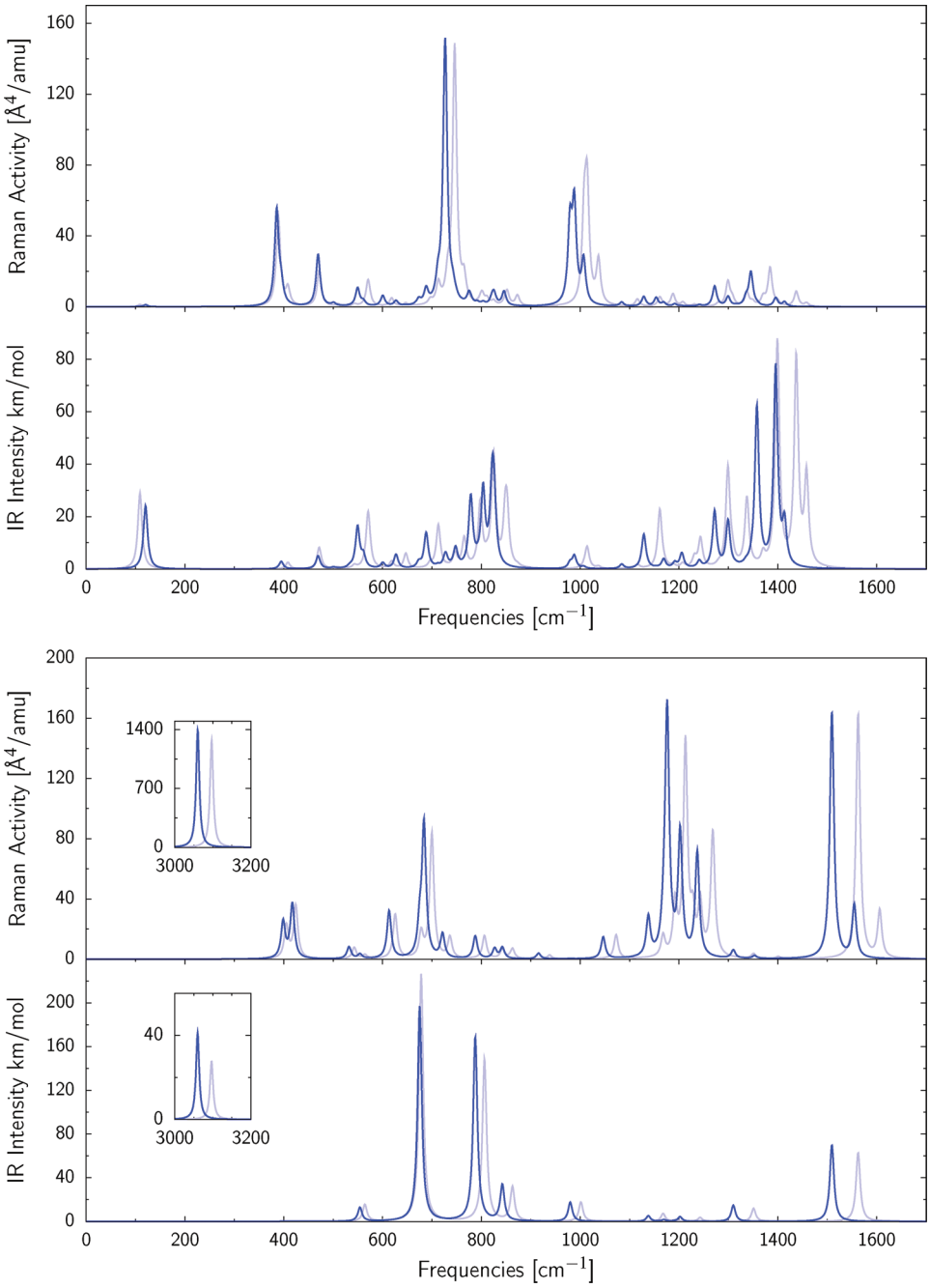


**Figure 4.** IR and Raman spectra of Ti@$C_{28}$ (top) and $C_{28}H_4$ (bottom) computed within harmonic approximation using B3LYP (dark blue lines) and CAM-B3LYP (light blue lines) methods and 6-31+G(d,p) basis set. The insets show the C−H stretching bands above 3000 $cm^{-1}$ that are present only in $C_{28}H_4$.

employed, and the usual scaling factors were used for the harmonic frequencies. The good performance of B3LYP for IR intensities[89] and Raman activities[90] in comparison with high-level ab initio results has also been reported by Halls and Schlegel. Thus, we may assume that the results reported here are reasonably accurate.

The B3LYP and CAM-B3LYP harmonic frequencies for Ti@$C_{28}$ are in good agreement. The root-mean-square (rms) deviation between the unscaled frequencies is 27.8 $cm^{-1}$ (the corresponding average absolute deviation of CAM-B3LYP with respect to B3LYP is 1.5%) with a maximum absolute difference (MAD) of 44.6 $cm^{-1}$. (The rms deviation was computed, as in ref 88, between symmetry-matched modes and degenerate modes were counted only once.) For $C_{28}H_4$ the rms deviation is quite similar, namely 27.2 $cm^{-1}$ (2.1%), with a MAD of 53.9 $cm^{-1}$. Generally, the discrepancies are larger at higher frequencies.

In the $C_{3v}$ point group of Ti@$C_{28}$ the modes of $a_1$ and e symmetry are both Raman and IR allowed. At the DFT level, the largest IR intensities are carried by the two high-frequency modes of e symmetry at 1357 and 1396 (1399 and 1437) $cm^{-1}$ at the B3LYP (CAM-B3LYP) levels. In addition, a cluster of four average intensity modes is found in the range 780−830 (765−852) $cm^{-1}$.

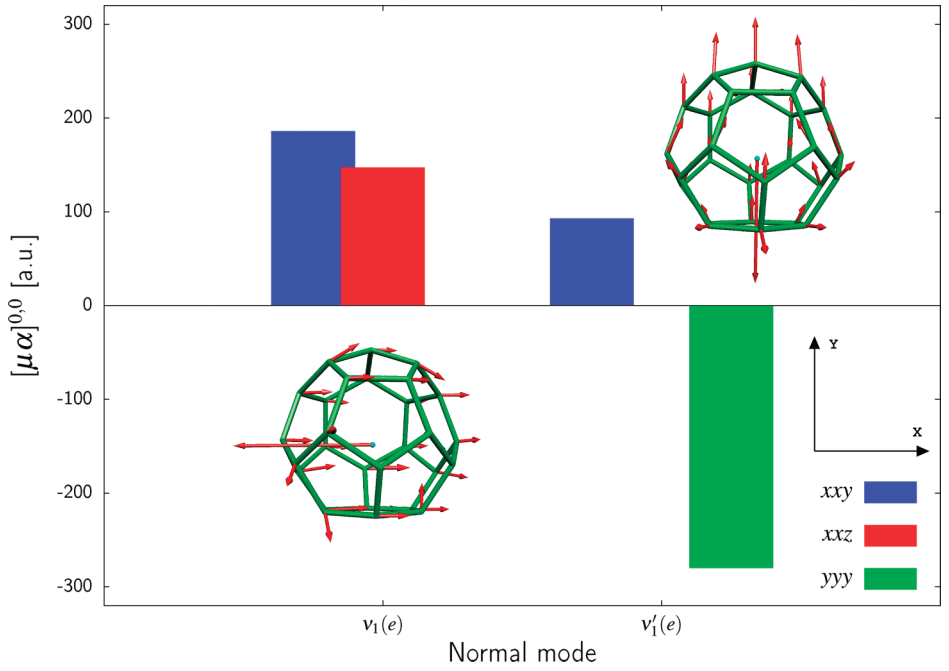


**Figure 5.** The two components of the low-frequency e symmetry normal mode of $Ti@C_{28}$ discussed in the text and their contributions to the tensor elements of $[\overline{\mu\alpha}]^{0,0}$. Please note that the orientation of the molecular frame is different from that in Figure 2 and the principal $C_3$ ($z$) axis now goes through the carbon atom closest to the reader.

The mode of lowest frequency, which occurs at 118 (108) $cm^{-1}$ and has e symmetry, may be described as a "rattling" of the Ti atom in the cage. It carries a fairly large IR intensity of 12.2 (14.6) km/mol, which is roughly the same as the intensity of the modes at 780−830 (765−852) $cm^{-1}$. For $C_{28}H_4$, only modes of $t_2$ symmetry are IR allowed, leading to a comparatively simple spectrum with the two strongest peaks at 674 (677) and 787 (806) $cm^{-1}$.

By far the strongest Raman active vibration of $Ti@C_{28}$ is the cage breathing mode of $a_1$ symmetry that occurs at 726 (745) $cm^{-1}$ in the B3LYP (CAM-B3LYP) calculation. The corresponding mode of $C_{28}H_4$ is shifted to 683 (699) $cm^{-1}$. Next most intense for $Ti@C_{28}$ (about 3.5 times weaker) is another $a_1$ mode at 979 (1008) $cm^{-1}$. The corresponding $a_1$ mode of $C_{28}H_4$ is shifted to higher frequencies: 1175 (1212) $cm^{-1}$ with a significant increase of Raman activity (nearly 4 times). One should note, however, that the Raman spectrum of $C_{28}H_4$ is dominated by the nearly degenerate $t_2$ and $a_1$ hydrogen stretching frequencies at 3060 (∼3100) $cm^{-1}$.

As far as the vibrational contribution to the electric properties of $Ti@C_{28}$ is concerned, the most relevant difference between the endohedral and exohedral species is the low-frequency degenerate e symmetry vibration of the former associated with large displacements of Ti within the cage, even though the Raman activity of this mode is quite weak (see below).

**Clamped Nucleus Electronic Contributions to Electrical Properties of $Ti@C_{28}$.** The coordinate system employed for electrical property calculations of the $Ti@C_{28}$ complex in $C_{3v}$ symmetry is shown in Figures 2 and 5 (the Cartesian coordinates are provided in the Supporting Information). The $z$-axis is collinear with the principal $C_3$ symmetry axis, and the Ti atom is at a distance of 0.4579 Å from an origin placed at the center of nuclear charge (or 0.4533 Å from the center of mass). This equilibrium geometry is in good agreement with the results of Dunlap et al.[51]

In Table 4 we present the diagonal components of the static electronic dipole moment and linear polarizability, as well as the first and second hyperpolarizabilities of $C_{28}$, $C_{28}H_4$, and $Ti@C_{28}$ at the equilibrium geometry. Except, perhaps, for the linear polarizability we see that electron correlation, estimated at the MP2 level, often has a significant effect on the computed property. For $C_{28}$ two structures were investigated. The first is the true equilibrium $T_d$ structure, while the second is the geometry this moiety assumes in the $Ti@C_{28}$ endohedral complex of $C_{3v}$ symmetry. The reduction in symmetry for the latter leads to a nonzero average first hyperpolarizability. It also leads to an increase in the diagonal components of $\gamma$ (ROMP2 level). (Note that $\beta_{xxx} = 0$ is not a consequence of symmetry but rather of the (arbitrary) choice for the direction of the $x$-axis.)

Whereas encapsulation of Ti into the $C_{3v}$ configuration of $C_{28}$ leads to a small change in the linear polarizability, there is a large reduction in the magnitude of the hyperpolarizabilities (MP2 level). This has been rationalized in other cases by invoking the orbital contraction (compression) effect.[91−94] On the other hand, we prefer an explanation based on the bonding interaction, and consequent localization, involving the four unpaired electrons within the $C_{28}$ cage. A comparison with $C_{28}H_4$ indicates that similar behavior is observed even though there can be no compression effect in that case.

**Vibrational Contributions to Electrical Properties of $Ti@C_{28}$.** In Table 5 we present several of the square bracket double harmonic vibrational contributions to the static (hyper)-polarizabilities of $Ti@C_{28}$. The static electronic (hyper)-polarizabilities are also included for comparison purposes. The values of the electronic properties obtained at the RHF level differ from those in Table 4 because different structures were used for the calculations. That is, the RMP2/6-31G(d) geometry was used for the data of Table 4, while the properties in Table 5 were calculated using geometries optimized at the same level of theory as the property calculations. This is necessary in order to correctly evaluate the vibrational (hyper)polarizabilities.

**Table 4. Static Diagonal Components of the Electronic Electric Dipole Moment and (Hyper)polarizabilities[a] (in au) of Ti@$C_{28}$, $C_{28}H_4$, and Two Structures of $C_{28}$[b]**

| | Ti@$C_{28}$ ($C_{3v}$) | | $C_{28}$ ($C_{3v}$)[c] | | $C_{28}$ ($T_d$) | | $C_{28}H_4$ ($T_d$) | |
|---|---|---|---|---|---|---|---|---|
| | RHF | RMP2 | ROHF | ROMP2 | ROHF | ROMP2 | RHF | RMP2 |
| $\mu_x$ | 0.000 | 0.000 | 0.000 | 0.000 | 0.000 | 0.000 | 0.000 | 0.000 |
| $\mu_z$ | 1.612 | 1.088 | −0.009 | −0.055 | 0.000 | 0.000 | 0.000 | 0.000 |
| $\alpha_{xx}$ | 267.20 | 275.96 | 254.92 | 277.40 | 251.33 | 265.30 | 246.59 | 251.06 |
| $\alpha_{zz}$ | 245.81 | 258.83 | 258.94 | 281.04 | 251.33 | 265.30 | 246.59 | 251.06 |
| $\beta_{xxx}$ | 0.0 | 0.0 | 0.0 | 0.0 | 0.0 | 0.0 | 0.0 | 0.0 |
| $\beta_{yyy}$ | −33.9 | −126.6 | −40.6 | −192.0 | 0.0 | 0.0 | 0.0 | 0.0 |
| $\beta_{zzz}$ | 117.3 | 23.1 | −92.0 | −588.4 | 0.0 | 0.0 | 0.0 | 0.0 |
| $\gamma_{xxxx} \times 10^{-3}$ | 96.2 | 119.5 | 101.8 | 149.6 | 96.6 | 127.0 | 72.0 | 104.0 |
| $\gamma_{zzzz} \times 10^{-3}$ | 79.3 | 103.7 | 99.9 | 141.2 | 96.6 | 127.0 | 72.0 | 104.0 |

[a] For the systems studied, and axes as defined, $\mu_y = \mu_x$, $\alpha_{yy} = \alpha_{xx}$, and $\gamma_{yyyy} = \gamma_{xxxx}$. [b] These values were estimated using the Rutishauser−Romberg procedure and 6-31+G(d,p) basis set. [c] Carbon cage geometry corresponding to rigid removal of Ti from Ti@$C_{28}$.

The data in Table 5 reveal some significant scatter among the various methods used to calculate the double harmonic vibrational terms. It is not straightforward to attribute the differences in DFT values to a specific feature of the exchange-correlation (xc) potential, particularly when the choice of basis set is as important as it is here. However, it is noticeable that for $[\overline{\mu^2}]$ and $[\overline{\mu\alpha}]$ the BLYP/6-31+G(d) and B3LYP/6-31+G(d) values are quite close to one another but differ substantially from the corresponding CAM-B3LYP value. On the basis of other systems[95] one might expect the CAM-B3LYP functional to be the preferred choice, but that is by no means definitive. Our results do suggest that, for these properties (and this system), the treatment of long-range exchange is important. On the other hand, the $[\overline{\alpha^2}]$ term is, surprisingly, almost independent of the xc functional.

For the first hyperpolarizability the double harmonic vibrational contribution to the average value (6-31+G(d) basis set) is much larger than the static electronic term. The largest contributions to $[\overline{\mu\alpha}]^{0,0}_{\omega=0}$ are due to the *xxy*, *xxz*, and *yyy* components which, in turn, are dominated by the lowest-frequency degenerate pair of e symmetry vibrations shown in Figure 5. For instance, the B3LYP/6-31+G(d) value for the tensor element $[\mu\alpha]^{0,0}_{xxz}$ is 149 au while the corresponding contribution from the e symmetry pair (at 120 $cm^{-1}$) is 147 au. On the other hand, the largest contribution to $[\overline{\mu\alpha}]^{0,0}$ is due to the *yyy* component (the B3LYP/6-31+G(d) value is −341 au), which is also largely determined by the two components of the e symmetry pair (the corresponding contribution to $[\mu\alpha]^{0,0}_{yyy}$ is −280 au). The e vibration in question involves a particularly large displacement of the Ti atom with respect to the cage in the *xy* plane (in Figure 5 the two components have arbitrarily been oriented in the *x* and *y* directions). The potential energy surface for these modes is very shallow. To illustrate that point, the B3LYP/6-31+G(d) energy profile for normal mode displacements of the e symmetry vibration is contrasted in Figure 6 with that of the $\nu_3(a_1)$ mode of frequency 394 $cm^{-1}$. The latter was chosen for this purpose because the normal mode displacements of the Ti atom (in this case along the $C_3$ axis) are also large.

In comparison with IR and Raman vibrational intensities, the double harmonic expressions for vibrational (hyper)polarizabilities contain an additional weighting factor of (frequency)$^{-2}$. That is why the vibrational modes corresponding to intense spectral features present in Figure 4 make relatively minor contributions to the double harmonic vibrational hyperpolarizabilities. It also explains why the 120 $cm^{-1}$ e symmetry mode can make the dominant

**Table 5. Static Electronic and Double Harmonic Vibrational Terms That Contribute to the (Hyper)polarizability[a] of Ti@$C_{28}$ (in au), As Calculated by the RHF and Several DFT Methods Using the 6-31+G(d) and 6-31G(d) (Values in Square Brackets) Basis Sets[b]**

| | BLYP | B3LYP | CAM-B3LYP | RHF |
|---|---|---|---|---|
| $\alpha^e_{xx}$ | 272.0 | 264.4 | 258.7 | 258.4 |
| $\alpha^e_{zz}$ | 259.9 | 250.0 | 241.8 | 238.6 |
| $\bar{\alpha}^e$ | 267.9 | 259.6 | 253.1 | 251.8 |
| | [229.1] | [223.6] | [218.3] | [216.6] |
| $[\mu^2]^{0,0}_{xx,\omega=0}$ | 21.2 | 27.1 | 38.0 | 58.1 |
| $[\mu^2]^{0,0}_{zz,\omega=0}$ | 4.2 | 3.9 | 3.8 | 4.7 |
| $[\overline{\mu^2}]^{0,0}_{\omega=0}$ | 15.5 | 19.3 | 26.5 | 40.3 |
| | [9.7] | [13.9] | [20.4] | [34.9] |
| $\beta^e_{xxx}$ | 0.0 | 0.0 | 0.0 | 0.0 |
| $\beta^e_{yyy}$ | −71.2 | −65.7 | −66.6 | −66.5 |
| $\beta^e_{zzz}$ | 4.3 | 25.5 | 61.3 | 98.6 |
| $\bar{\beta}^e$ | 7.6 | −10.4 | −14.1 | −34.4 |
| | [−360.6] | [−347.2] | [−333.5] | [−345.1] |
| $[\mu\alpha]^{0,0}_{xxx,\omega=0}$ | 0.0 | 0.0 | 0.0 | 0.0 |
| $[\mu\alpha]^{0,0}_{yyy,\omega=0}$ | −273.5 | −341.4 | −448.5 | −673.0 |
| $[\mu\alpha]^{0,0}_{zzz,\omega=0}$ | 6.5 | 27.4 | 43.1 | 69.4 |
| $[\overline{\mu\alpha}]^{0,0}_{\omega=0}$ | 196.2 | 195.3 | 275.9 | 175.4 |
| | [223.9] | [277.0] | [417.6] | [438.6] |
| $\gamma^e_{xxxx}$ | $110 \times 10^3$ | $98 \times 10^3$ | $85 \times 10^3$ | $94 \times 10^3$ |
| $\gamma^e_{zzzz}$ | $92 \times 10^3$ | $81 \times 10^3$ | $70 \times 10^3$ | $74 \times 10^3$ |
| $\bar{\gamma}^e$ | $103 \times 10^3$ | $91 \times 10^3$ | $79 \times 10^3$ | $87 \times 10^3$ |
| | $[6 \times 10^3]$ | $[6 \times 10^3]$ | $[5 \times 10^3]$ | $[7 \times 10^3]$ |
| $[\alpha^2]^{0,0}_{xxxx,\omega=0}$ | $24 \times 10^3$ | $23 \times 10^3$ | $22 \times 10^3$ | $23 \times 10^3$ |
| $[\alpha^2]^{0,0}_{zzzz,\omega=0}$ | $18 \times 10^3$ | $16 \times 10^3$ | $14 \times 10^3$ | $14 \times 10^3$ |
| $[\overline{\alpha^2}]^{0,0}_{\omega=0}$ | $21 \times 10^3$ | $19 \times 10^3$ | $19 \times 10^3$ | $19 \times 10^3$ |
| | $[17 \times 10^3]$ | $[15 \times 10^3]$ | $[15 \times 10^3]$ | $[15 \times 10^3]$ |

[a] For the systems studied, and the definition of axes, $\alpha^e_{yy} = \alpha^e_{xx}$, $[\mu^2]^{0,0}_{yy,\omega=0} = [\mu^2]^{0,0}_{xx,\omega=0}$, $\gamma^e_{yyyy} = \gamma^e_{xxxx}$, and $[\alpha^2]^{0,0}_{yyyy,\omega=0} = [\alpha^2]^{0,0}_{xxxx,\omega=0}$. [b] All calculations in this table were performed at the geometry obtained from the corresponding quantum chemical method.

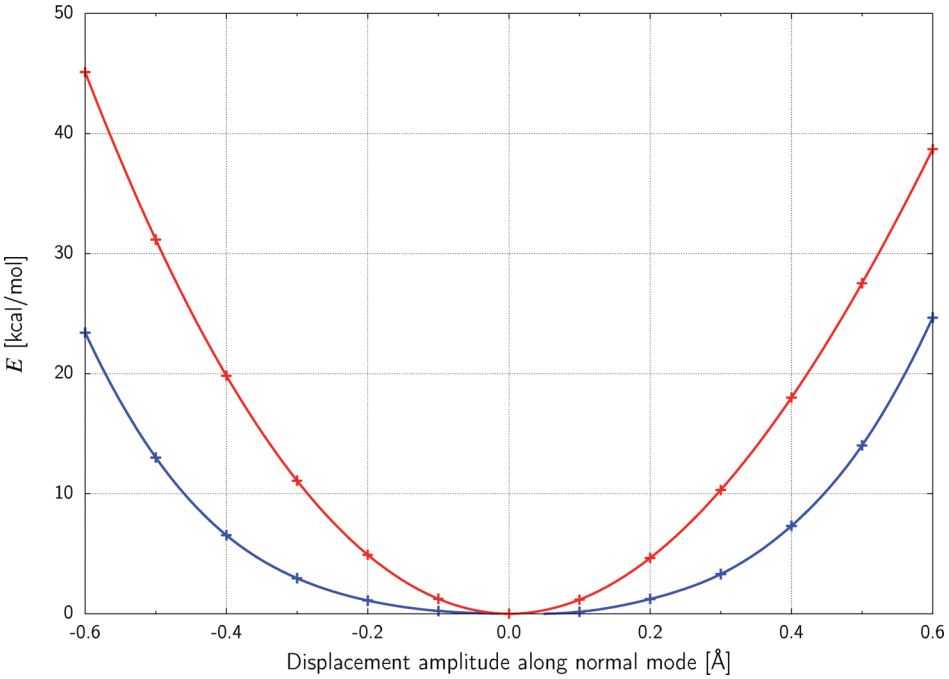


**Figure 6.** Variation of B3LYP/6-31+G(d) energy for Ti@$C_{28}$ as a function of the displacement of atoms from the equilibrium geometry along the selected low-frequency normal modes characterized by large amplitudes of Ti atom motions along the principal symmetry axis ($\nu_3(a_1)$, red) and in the perpendicular *xy* plane (doubly degenerate $\nu_1$(e), blue).

contribution to the first hyperpolarizability despite its very small Raman activity (0.6 Å$^4$/amu) and why the 394 cm$^{-1}$ $a_1$ symmetry vibration is not more important, even though the corresponding product of IR intensity (2.8 km/mol) and Raman activity (9.6 Å$^4$/amu) is larger. It is reasonable to assume that the low-frequency modes that dominate the double harmonic term will also make large anharmonicity contributions. Indeed, we have computed $\beta^{nr}_{yyy}$ at the B3LYP/6-31+G(d) level of theory and it turns out to be $2.0 \times 10^3$ au, which is several times larger than the double harmonic value and is associated with displacement of Ti along the *y* axis that is an order of magnitude larger than for any of the carbon atoms.

Contrary to the case of the first hyperpolarizability, $\beta$, the double harmonic contribution to the components of the static $\alpha$ and $\gamma$ ($[\alpha^2]$ term) is much smaller than the corresponding electronic contribution. Nevertheless, the very large anharmonic contribution to $\beta$, which is a consequence of the flat PES landscape of Ti@$C_{28}$, suggests that the complete vibrational contribution to $\gamma$ may be far larger than the double harmonic $[\alpha^2]$ term.

In addition to nuclear relaxation there is a pure vibrational contribution to the (hyper)polarizabilities that arises from higher order anharmonic effects, which is known as the c-zpva term. Again, because of the very flat PES, this term *may* be very large. However, its calculation presents some difficulties since the detailed shape of the PES with its four equivalent minima must be explicitly taken into account. Some of us have developed a new procedure for obtaining the c-zpva contribution in molecules with double minima,[96] and we are currently working on the generalization to *n* equivalent minima. When that is done we plan to apply the new procedure to Ti@$C_{28}$.

It is of interest to compare the results found here with those obtained recently for Li@$C_{60}$. In both cases the double harmonic vibrational contribution to the static linear polarizability is small compared to the pure electronic term. On the other hand, for Li@$C_{60}$ the nuclear relaxation contributions to the static first and second hyperpolarizabilities are quite large.[45] This is consistent with what we have found for the static first hyperpolarizability of Ti@$C_{28}$. For the second hyperpolarizability only the $[\alpha^2]^{0,0}$ double harmonic term has been evaluated here. Although a more thorough comparison of the two endohedral fullerenes is desirable, it is beyond the scope of this paper and, indeed, is not feasible at the moment for several reasons: (i) a more extensive exploration of the Li@$C_{60}$ PES, as done here for Ti@$C_{28}$, is required; (ii) the level of theory applied thus far is different in the two cases; (iii) a more complete treatment of anharmonicity, taking into account the c-zpva contribution, should be included.

## CONCLUSIONS

We have determined the structure, dipole moment, and (hyper)polarizabilities of $C_{28}$ and Ti@$C_{28}$ at various levels of approximation (HF, DFT, R(O)MP2). An "atoms in molecules" analysis of the interaction between the embedded Ti atom and the $C_{28}$ cage was carried out and the UV−vis, IR, and Raman spectra were calculated for this endohedral fullerene. In addition, both electronic and (double harmonic) vibrational contributions to the static polarizability and hyperpolarizabilities were evaluated.

The major findings of the present work are as follows. Encapsulation of Ti in $C_{28}$ lowers the symmetry from $T_d$ to $C_{3v}$. There are transition states of $C_{2v}$ and $C_{3v}$ symmetry connecting the four equivalent minima that lie 2.3 and 7.1 kcal/mol, respectively, above the global minimum in MP2/6-31G(d) calculations. The position at the center of the cage is a third-order transition state. It connects the six $C_{2v}$ stationary points and lies 45.5 kcal/mol above them at the same MP2/6-31G(d) level of treatment. Our calculations confirm previous reports indicating that the endohedral complex is very stable: a binding energy of 181.3 kcal/mol is found for Ti@$C_{28}$ at the ROMP2/6-31G(d)

level. Topological analysis of the generalized MP2 density reveals four bond paths between Ti and carbon atoms of the host corresponding to a partially covalent closed shell interaction.

The reduced symmetry of the fullerene cage due to encapsulation causes an increase in the diagonal components of the static electronic linear polarizability and second hyperpolarizability as well as nonzero values for the dipole moment and first hyperpolarizability. On the other hand, introduction of the Ti atom leads to localized bonding interactions and a consequent comparable or larger reduction in most cases for electrical properties other than the dipole moment.

Our preliminary B3LYP/6-31+G(d) calculations reveal that, in the double harmonic approximation, the static vibrational average first hyperpolarizability is much (5 times) larger than its electronic counterpart. When anharmonicity is considered, the corresponding nuclear relaxation contribution to the major component is much larger than the double harmonic term (6 times). Otherwise, our calculations indicate that the double harmonic vibrational linear polarizability is relatively small compared to its pure electronic counterpart as is the $[\alpha^2]$ contribution to the second hyperpolarizability. Nevertheless, the flat potential energy surface, and the resulting very large anharmonic contribution to the first hyperpolarizability, indicates that the vibrational $\gamma$ may exceed the corresponding electronic term when anharmonicity is taken into account. In addition to nuclear relaxation, the higher order c-zpva contribution may also be very substantial. On the basis of our treatment of double minimum potentials[96] we are currently developing methodology that will enable us to calculate this contribution for $Ti@C_{28}$, which has a PES with four equivalent minima that are separated by low energy barriers.

Since we believe that $Ti@C_{28}$ might be of interest for further experimental and theoretical studies, we have carried out an extensive spectroscopic characterization including UV−vis, IR, and Raman spectra estimated using the KS-DFT approach with a selection of functionals including BLYP, B3LYP, and CAM-B3LYP. An analysis of the effect of encapsulation was done by comparing $Ti@C_{28}$ with $C_{28}H_4$.

## ■ ASSOCIATED CONTENT

**Supporting Information.** Cartesian coordinates of the stationary points, a more detailed plot of the calculated UV−vis spectrum, details of the calculated IR and Raman spectra, and the molecular graph of $Ti@C_{28}$. This material is available free of charge via the Internet at http://pubs.acs.org.

## ■ AUTHOR INFORMATION

### Corresponding Authors

*E-mail: robert.gora@pwr.wroc.pl (R.W.G.); mpapad@eie.gr (M.G.P.); kirtman@chem.ucsb.edu (B.K.).

## ■ ACKNOWLEDGMENT

The support from the European Union (MTKD-CT-2006-042488), and the computing resources from the Barcelona Supercomputing Center, TeraGrid (USA), DEISA (seventh Framework Programme), and Wroclaw Center for Networking and Supercomputing are gratefully acknowledged. One of the authors (R.Z.) is the recipient of the fellowship cofinanced by the European Union within the European Social Fund. R.Z. would also like to acknowledge support from a grant from Iceland, Liechtenstein, and Norway through the EEA Financial Mechanism—Scholarship and Training Fund. M.G.P. wishes to acknowledge funding received from the European Union's Seventh Framework Programme (FP7-REGPOT-2009-1) under Grant Agreement No. 245866, and the High-Performance Computing Infrastructure for South East Europe's Research Communities (HP-SEE), a project cofunded by the European Commission (under Contract No. 261499) through the Seventh Framework Programme.

## ■ REFERENCES

(1) Heath, J. R.; O'Brien, S. C.; Zhang, Q.; Liu, Y.; Curl, R. F.; Kroto, H. W.; Tittel, F. K.; Smalley, R. E. *J. Am. Chem. Soc.* **1985**, *107*, 7779–7780.

(2) Kroto, H. W.; Heath, J. R.; O'Brien, S. C.; Curl, R. F.; Smalley, R. E. *Nature* **1985**, *318*, 162–163.

(3) Chai, Y.; Guo, T.; Jin, C. M.; Haufler, R. E.; Chibante, L. P. F.; Fure, J.; Wang, L.; Alford, M.; Smalley, R. E. *J. Phys. Chem.* **1991**, *95*, 7564–7568.

(4) Nagase, S.; Kobayashi, K.; Akasaka, T.; Wakahara, T. In *Fullerenes: Chemistry, Physics, and Technology*; Kadish, K. M., Ruoff, R. S., Eds.; John Wiley and Sons: New York, 2000; pp 395−436.

(5) *Endofullerenes: A New Family of Carbon Clusters*; Akasaka, T., Nagase, S., Eds.; Kluwer Academic Publishers: Dordrecht, The Netherlands, 2002.

(6) Shinohara, H. *Rep. Prog. Phys.* **2000**, *63*, 843–892.

(7) Campbell, E.; Fanti, M.; Hertel, I.; Mitzner, R.; Zerbetto, F. *Chem. Phys. Lett.* **1998**, *288*, 131–137.

(8) Gu, G.; Huang, H.; Yang, S.; Yu, P.; Fu, J.; Wong, G.; Wan, X.; Dong, J.; Du, Y. *Chem. Phys. Lett.* **1998**, *289*, 167–173.

(9) Campbell, E. E. B.; Couris, S.; Fanti, M.; Koudoumas, E.; Krawez, N.; Zerbetto, F. *Adv. Mater.* **1999**, *11*, 405–408.

(10) Antoine, R.; Rayane, D.; Benichou, E.; Dugourd, P.; Broyer, M. *Eur. Phys. J. D* **2000**, *12*, 147–151.

(11) Torrens, F. *Nanotechnology* **2002**, *13*, 433–438.

(12) Torrens, F. *J. Phys. Org. Chem.* **2002**, *15*, 742–749.

(13) Xenogiannopoulou, E.; Couris, S.; Koudoumas, E.; Tagmatarchis, N.; Inoue, T.; Shinohara, H. *Chem. Phys. Lett.* **2004**, *394*, 14–18.

(14) Tang, C.; Deng, K.; Tan, W.; Yuan, Y.; Liu, Y.; Wu, H.; Huang, D.; Hu, F.; Yang, J.; Wang, X. *Phys. Rev. A* **2007**, *76*, 013201.

(15) Yan, H.; Yu, S.; Wang, X.; He, Y.; Huang, W.; Yang, M. *Chem. Phys. Lett.* **2008**, *456*, 223–226.

(16) Yaghobi, M.; Rafie, R.; Koohi, A. *THEOCHEM* **2009**, *905*, 48–50.

(17) He, J.; Wu, K.; Sa, R.; Li, Q.; Wei, Y. *Chem. Phys. Lett.* **2009**, *475*, 73–77.

(18) Chai, Y.; Guo, T.; Jin, C.; Haufler, R. E.; Chibante, L. P. F.; Fure, J.; Wang, L.; Alford, J. M.; Smalley, R. E. *J. Phys. Chem.* **1991**, *95*, 7564.

(19) Manolopoulous, D. E.; Fowler, P. W. *Chem. Phys. Lett.* **1991**, *187*, 12.

(20) Bethune, D. S.; Johnson, R. D.; Salem, J. R.; de Vries, M. S.; Yannoni, C. S. *Nature* **1993**, *366*, 123.

(21) Beyers, R.; Kiang, C. H.; Johnson, R. D.; Salem, J. R.; de Vries, M. S.; Yannoni, C. S.; Bethune, D. S.; Dorn, H. C.; Burbank, P.; Harich, K.; Stevenson, S. *Nature* **1994**, *370*, 196.

(22) Fowler, P.; Manoloupoulos, D. E. *An Atlas of Fullerenes*; Oxford University Press: Oxford, U.K., 1995.

(23) Kobayashi, K.; Nagase, S. *Chem. Phys. Lett.* **1996**, *262*, 227.

(24) Saunders, M.; Cross, R. J.; Jimenez Vazquez, H. A.; Shimshi, R.; Khong, A. *Science* **1996**, *271*, 1693–1697.

(25) Guha, S.; Nakamoto, K. *Coord. Chem. Rev.* **2005**, *249*, 1111.

(26) Dunsch, L.; Yang, S. *Electrochem. Soc. Interface* **2006**, *15*, 34.

(27) Rehaman, A.; Gagliardi, L.; Pyykkö, P. *Int. J. Quantum Chem.* **2007**, *107*, 1162.

(28) Infante, I.; Gagliardi, L.; Scuseria, G. E. *J. Am. Chem. Soc.* **2008**, *130*, 7459.

(29) Cioslowski, J.; Fleischmann, E. D. *J. Chem. Phys.* **1991**, *94*, 3730–3734.
(30) Cioslowski, J. *J. Am. Chem. Soc.* **1991**, *113*, 4139–4141.
(31) Ross, M. M.; Nelson, H. H.; Callahan, J. H.; McElvany, S. W. *J. Phys. Chem.* **1992**, *96*, 5231.
(32) Campanera, J. M.; Bo, C.; Olmstead, M. M.; Balch, A. L.; Poblet, J. M. *J. Phys. Chem. A* **2002**, *106*, 12356.
(33) Nadaï, C. D.; Mirone, A.; Dhesi, S. S.; Bencok, P.; Brookes, N. B.; Marenne, I.; Rudolf, P.; Tagmatarchis, N.; Shinohara, H.; Dennis, T. J. S. *Phys. Rev. B* **2004**, *69*, 184421.
(34) Park, S. S.; Liu, D.; Hagelberg, F. *J. Phys. Chem. A* **2005**, *109*, 8865.
(35) Luo, Y.; Norman, P.; Macak, P.; Ågren, H. *Phys. Rev. B* **2000**, *61*, 3060.
(36) Jensen, L.; Åstrand, P. O.; Mikkelsen, K. V. *J. Phys. Chem. B* **2004**, *108*, 8226.
(37) Xie, R. H.; Rao, Q.; Jensen, L. In *Encyclopedia of Nanoscience and Nanotechnology*; Nalwa, H. S., Ed.; American Scientific: Stevenson Ranch, CA, USA, 2004; p 67.
(38) Jensen, L.; Åstrand, P. O.; Osted, A.; Kongsted, J.; Mikkelsen, K. V. *J. Chem. Phys.* **2002**, *116*, 4001.
(39) van Gisbergen, S. J. A.; Snijders, J. G.; Baerends, E. J. *Phys. Rev. Lett.* **1997**, *78*, 3097.
(40) Jonsson, D.; Norman, P.; Ruud, K.; Ågren, H. *J. Chem. Phys.* **1998**, *109*, 572.
(41) Talapatra, G. B.; Manickam, N.; Samoć, M.; Orczyk, M.; Karna, S. P.; Prasad, P. N. *J. Phys. Chem.* **1992**, *96*, 5206.
(42) Thole, B. T. *Chem. Phys.* **1981**, *59*, 341.
(43) Jensen, L.; van Duijnen, P. T. *Int. J. Quantum Chem.* **2005**, *102*, 612.
(44) Whitehouse, D. B.; Buckingham, A. D. *Chem. Phys. Lett.* **1993**, *207*, 332.
(45) Reis, H.; Loboda, O.; Avramopoulos, A.; Papadopoulos, M. G.; Kirtman, B.; Luis, J. M.; Zaleśny, R. *J. Comput. Chem.* **2010**, *32*, 908–914.
(46) Guo, T.; Diener, M.; Cai, Y.; Alford, M. J.; Haufler, R. E.; McClure, S. M.; Ohno, T.; Weaver, J. H.; Scuseria, G. E.; Smalley, R. E. *Science* **1992**, *257*, 1661.
(47) Guo, T.; Smalley, R. E.; Scuseria, G. E. *J. Chem. Phys.* **1993**, *99*, 352.
(48) Fayereisen, M.; Gutowski, M.; Simons, J.; Almlöf, J. *J. Chem. Phys.* **1992**, *96*, 2926.
(49) Zhao, X.; Lu, P.; Hao, C.; Li, S.; Qiu, J. *THEOCHEM* **2006**, *760*, 53–57.
(50) Makurin, Y. N.; Sofronov, A. A.; Gusev, A. I.; Ivanovsky, A. L. *Chem. Phys.* **2001**, *270*, 293.
(51) Dunlap, B. I.; Häberlen, O. D.; Rösch, N. *J. Phys. Chem.* **1992**, *96*, 9095.
(52) Häberlen, O. D.; Rösch, N.; Dunlap, B. I. *Chem. Phys. Lett.* **1992**, *200*, 418.
(53) McWeeny, R.; Diercksen, G. *J. Chem. Phys.* **1968**, *49*, 4852–4856.
(54) Zhao, K.; Pitzer, R. M. *J. Phys. Chem.* **1996**, *100*, 4798.
(55) Glaesemann, K. R.; Schmidt, M. W. *J. Phys. Chem. A* **2010**, *114*, 8772–8777.
(56) Colvin, M.; Janssen, C.; Seidl, E.; Nielsen, I.; Melius, C. *Chem. Phys. Lett.* **1998**, *287*, 537–541.
(57) Smith, S.; Markevitch, A.; Romanov, D.; Li, X.; Levis, R.; Schlegel, H. *J. Phys. Chem. A* **2004**, *108*, 11063–11072.
(58) Champagne, B.; Botek, E.; Nakano, M.; Nitta, T.; Yamaguchi, K. *J. Chem. Phys.* **2005**, *122*, 114315.
(59) Bauschlicher, C. W. *Theor. Chem. Acc.* **2003**, *110*, 153–155.
(60) Rutishauser, H. *Numer. Math.* **1963**, *5*, 48–54.
(61) Kurtz, H. A.; Stewart, J. J. P.; Dieter, K. M. *J. Comput. Chem.* **1990**, *11*, 82.
(62) O'Boyle, N. M.; Tenderholt, A. L.; Langner, K. M. *J. Comput. Chem.* **2008**, *29*, 839–845.
(63) Bishop, D. *Adv. Chem. Phys.* **1998**, *104*, 1–40.
(64) Kirtman, B.; Luis, J. In *Non-Linear Optical Properties of Matter, From Molecules to Condensed Phases*; Papadopoulos, M., Sadlej, A., Leszczynski, J., Eds.; Springer: New York, 2006; pp 101−128.
(65) Kirtman, B.; Luis, J. M.; Bishop, D. M. *J. Chem. Phys.* **1998**, *108*, 10008.
(66) Torrent-Succarat, M.; Sola, M.; Duran, M.; Luis, J. M.; Kirtman, B. *J. Chem. Phys.* **2002**, *116*, 5363.
(67) Jug, K.; Chiodo, S.; Calaminici, P.; Avramopoulos, A.; Papadopoulos, M. G. *J. Phys. Chem. A* **2003**, *107*, 4172.
(68) Kirtman, B.; Champagne, B.; Luis, J. M. *J. Comput. Chem.* **2000**, *16*, 1572.
(69) Hansen, M. B.; Christiansen, O.; Hättig, C. *J. Chem. Phys.* **2009**, *131*, 154101.
(70) Kirtman, B.; Luis, J. M. *Int. J. Quantum Chem.* **2011**, *111*, 839.
(71) Bishop, D. M.; Hasan, M.; Kirtman, B. *J. Chem. Phys.* **1995**, *103*, 4157–4159.
(72) Luis, J. M.; Duran, M.; Andrés, J. L.; Champagne, B.; Kirtman, B. *J. Chem. Phys.* **1999**, *111*, 875–884.
(73) Becke, A. D. *Phys. Rev. A* **1988**, *38*, 3098–3100.
(74) Lee, C.; Yang, W.; Parr, R. G. *Phys. Rev. B* **1988**, *37*, 785–789.
(75) Yanai, T.; Tew, D. P.; Handy, N. C. *Chem. Phys. Lett.* **2004**, *393*, 51–57.
(76) Frisch, M. J.; et al. *Gaussian 09*, revision A.1; Gaussian Inc.: Wallingford, CT, USA, 2009.
(77) Schmidt, M. W.; Baldridge, K. K.; Boatz, J. A.; Elbert, S. T.; Gordon, M. S.; Jensen, J. H.; Koseki, S.; Matsunaga, N.; Nguyen, K. A.; Su, S.; Windus, T. L.; Dupuis, M.; Montgomery, J. A. *J. Comput. Chem.* **1993**, *14*, 1347–1363.
(78) Boys, S. F.; Bernardi, F. *Mol. Phys.* **1970**, *19*, 553–566.
(79) Bader, R. F. W. *Atoms In Molecules, A Quantum Theory*; Oxford University Press: Oxford, U.K., 1990.
(80) Bader, R. F. W. *Chem. Rev.* **1991**, *91*, 893.
(81) Popelier, P. *Atoms in Molecules, An Introduction*; Pearson Education Ltd.: Prentice Hall: New York, 2000.
(82) *The Quantum Theory of Atoms in Molecules: From Solid State to DNA and Drug Design*; Matta, C. F., Boyd, R. J., Eds.; Wiley-VCH: Weinheim, Germany, 2007.
(83) Biegler-Konig, F. *AIM2000* Package; University of Applied Sciences: Bielefeld, Germany.
(84) Espinosa, E.; Alkorta, I.; Elguero, J.; Molins, E. *J. Chem. Phys.* **2002**, *117*, 5529.
(85) Jackson, K.; Kaxiras, E.; Pederson, M. R. *Phys. Rev. B* **1993**, *48*, 17556.
(86) Bauernschmitt, R.; Ahlrichs, R.; Hennrich, F.; Kappes, M. *J. Am. Chem. Soc.* **1998**, *120*, 5052–5059.
(87) Hare, J. P.; Kroto, H. W.; Taylor, R. *Chem. Phys. Lett.* **1991**, *177*, 394.
(88) Jiménez-Hoyos, C. A.; Janesko, B. G.; Scuseria, G. E. *Phys. Chem. Chem. Phys.* **2008**, *10*, 6621.
(89) Halls, M. D.; Schlegel, H. B. *J. Chem. Phys.* **1998**, *109*, 10587.
(90) Halls, M. D.; Schlegel, H. B. *J. Chem. Phys.* **1999**, *111*, 8819.
(91) Papadopoulos, M. G.; Sadlej, A. J. *Chem. Phys. Lett.* **1998**, *288*, 377.
(92) Fowler, P. W.; Madden, P. A. *Phys. Rev. B* **1984**, *29*, 1035.
(93) Fowler, P. W. *J. Phys. Chem.* **1985**, *89*, 2581.
(94) Kaczmarek, A.; Bartkowiak, W. *Phys. Chem. Chem. Phys.* **2009**, *11*, 2885.
(95) Zaleśny, R.; Bulik, I. W.; Bartkowiak, W.; Luis, J. M.; Avramopoulos, A.; Papdopoulos, M. G.; Krawczyk, P. *J. Chem. Phys.* **2010**, *133*, 244308.
(96) Luis, J. M.; Reis, H.; Papadopoulos, M.; Kirtman, B. *J. Chem. Phys.* **2009**, *131*, 034116.